3rd International Conference on Mechanical Models in Structural Engineering
CMMoST 2015
24-26 June 2015 Seville SPAIN

Analysis of masonry vaults as a topology optimization problem

Bruggi, Matteo[1]; Taliercio, Alberto[2]

ABSTRACT

An innovative approach is proposed to analyze 3D masonry vaults, assuming masonry to behave as a linear elastic no-tension material. Masonry is replaced by a suitable equivalent orthotropic material with spatially varying elastic properties and negligible stiffness in any direction along which tensile stresses must be prevented. An energy-based algorithm is implemented to define the distribution and the orientation of the equivalent material for a given load, minimizing the potential energy so as to achieve a purely compressive state of stress. The algorithm is embedded within a numerical procedure that performs a non-incremental analysis under given loads. The collapse load of masonry structural elements can also be predicted running a sequence of independent analyses. The capabilities of the approach in predicting the crack pattern in typical masonry vaults are also shown.

Keywords: masonry vaults, linear elasticity, no-tension material, FEM, topology optimization.

1. INTRODUCTION

The collapse of masonry structures, especially arches and vaults, usually occurs far beyond first cracking. Accordingly, non-linear analyses are often preferred to conventional approaches based on the classic theory of elasticity when the safety of this type of structures has to be assessed. Limit analysis is widely adopted to evaluate the bearing capacity of ductile structures. Assuming the compressive strength of masonry to be infinite, neglecting its tensile strength and assuming "tensile strains" to be unbounded, limit analysis can be applied to evaluate the collapse load and the relevant failure mechanism(s) also for masonry structures. This approach has been extensively followed to investigate the structural behaviour of brickwork and stonework, in particular arches and vaults [1]. In principle, a full non-linear analysis is able to follow the complete loading process, from the initial stress-free state to the highly cracked state precursory of collapse. The reliability of the material models available so far is a crucial issue when the nonlinear analysis of existing masonry structures is carried out, see e.g. [2]. Among the approaches that are currently employed to analyse masonry-like solids, the no-tension model allows the structural behaviour to be evaluated assuming the stress tensor to be negative semi-definite and to depend linearly upon the elastic part of the strain, see e.g. [3]. The no-tension approach is of major importance since it allows the structural assessment to be performed both at the serviceability limit state and at incipient collapse, recovering conventional load multipliers computed through limit analysis. Notwithstanding the apparent simplicity of the no-tension model, the need to treat discontinuities in the stress and displacement fields gives rise to several numerical issues. Well-known difficulties arise when dealing with incremental approaches,

[1] *Department of Civil and Environmental Engineering. Politecnico di Milano (Italy).* matteo.bruggi@polimi.it
[2] *Department of Civil and Environmental Engineering. Politecnico di Milano (Italy).* alberto.taliercio@polimi.it *(Corresponding author)*

whereas robust energy-based procedures can be alternatively developed assuming no-tension bodies to be hyper-elastic [4].

This contribution extends the formulation originally presented in [5] for two-dimensional problems to three-dimensional ones. The real no-tension material is replaced by an equivalent orthotropic material, exhibiting negligible stiffness in any direction along which a tensile principal stress must be prevented in the body. The elasticities of the equivalent material along its symmetry axes are reduced with respect to those of the real material using a penalization law typical of Topology Optimization [6]. The equilibrium of the no-tension body is sought by minimizing the strain energy with respect to the distribution and the orientation of the orthotropic material.

A couple of case studies are presented to assess the proposed approach in the simulation of the structural response of three-dimensional no-tension structures. The collapse load multiplier of an arch subjected to an increasing horizontal force is computed and compared with the results given by limit analysis. The structural behaviour of a groin vault under dead loads is also investigated, comparing a conventional linear elastic analysis with the results of the proposed non-linear approach.

2. PROBLEM FORMULATION

2.1. Equivalent orthotropic material

Consider a 3D solid, consisting of an isotropic linear elastic no-tension material, occupying a domain Ω. The position of any point $\boldsymbol{\chi} \in \Omega$ is defined by a triplet of orthogonal Cartesian (global) coordinates, z_1, z_2, z_3. Let σ_α, α=I, II, III, be the eigenvalues of the stress tensor $\boldsymbol{\sigma}$ computed at $\boldsymbol{\chi}$, with $\sigma_\mathrm{I} \le \sigma_\mathrm{II} \le \sigma_\mathrm{III}$. According to the sign of the principal stresses, the material behaviour at $\boldsymbol{\chi}$ is different. If $\sigma_\mathrm{III} < 0$, the material behaves like a conventional isotropic material. If one or two of the principal stresses are positive, the material behaves like an orthotropic material: "cracking strains" $\varepsilon^c \ge 0$ arise along the tensile isostatic line(s), whereas the material behaves elastically along the direction(s) of the principal compressive stress(es). Finally, if $\sigma_\mathrm{I} \ge 0$, the material behaves like a "void phase", allowing for any positive semidefinite "cracking strain".

A suitable equivalent orthotropic material can be defined to match the behaviour of the real no-tension material according to the sign of the principal stresses. Let $\tilde{z}_i$, i=1,2,3, be the symmetry axes of the orthotropic material, locally coinciding with the principal stress directions z_α, α=I, II, III, at any point of the real solid. The stress-strain law for the orthotropic material at any point $\boldsymbol{\chi}$ can be written as $\tilde{\boldsymbol{\epsilon}} = \tilde{\boldsymbol{C}}\tilde{\boldsymbol{\sigma}}$, where, using the notation proposed in [7]:

$$\tilde{\boldsymbol{\epsilon}} = \begin{Bmatrix} \tilde{\epsilon}_{11} \\ \tilde{\epsilon}_{22} \\ \tilde{\epsilon}_{33} \\ \sqrt{2}\tilde{\epsilon}_{12} \\ \sqrt{2}\tilde{\epsilon}_{23} \\ \sqrt{2}\tilde{\epsilon}_{31} \end{Bmatrix}, \quad \tilde{\boldsymbol{\sigma}} = \begin{Bmatrix} \sigma_{11} \\ \tilde{\sigma}_{22} \\ \tilde{\sigma}_{33} \\ \sqrt{2}\tilde{\sigma}_{12} \\ \sqrt{2}\tilde{\sigma}_{23} \\ \sqrt{2}\tilde{\sigma}_{31} \end{Bmatrix} \tag{1}$$

and

$$\widetilde{\boldsymbol{C}} = \begin{bmatrix} 1/\tilde{E}_1 & -\tilde{\nu}_{21}/\tilde{E}_2 & -\tilde{\nu}_{31}/\tilde{E}_3 & 0 & 0 & 0 \\ -\tilde{\nu}_{12}/\tilde{E}_1 & 1/\tilde{E}_2 & -\tilde{\nu}_{32}/\tilde{E}_3 & 0 & 0 & 0 \\ -\tilde{\nu}_{13}/\tilde{E}_1 & -\tilde{\nu}_{23}/\tilde{E}_2 & 1/\tilde{E}_3 & 0 & 0 & 0 \\ 0 & 0 & 0 & 1/\tilde{G}_{12} & 0 & 0 \\ 0 & 0 & 0 & 0 & 1/\tilde{G}_{23} & 0 \\ 0 & 0 & 0 & 0 & 0 & 1/\tilde{G}_{31} \end{bmatrix}. \tag{2}$$

In eq. (2), $\tilde{E}_i$, *i*=1,2,3, is the Young's modulus of the equivalent material along the symmetry axis $\tilde{z}_i$, $\tilde{G}_{ij}$ *i,j*=1,2,3, is the shear modulus in the symmetry plane $(\tilde{z}_i, \tilde{z}_j)$ and $\tilde{\nu}_{ij}$, *i,j*=1,2,3, is the Poisson's ratio along $\tilde{z}_j$ under uniaxial tension along $\tilde{z}_i$. The equalities $\tilde{\nu}_{12}/\tilde{E}_1 = \tilde{\nu}_{21}/\tilde{E}_2$, $\tilde{\nu}_{13}/\tilde{E}_1 = \tilde{\nu}_{31}/\tilde{E}_3$ and $\tilde{\nu}_{23}/\tilde{E}_2 = \tilde{\nu}_{32}/\tilde{E}_{32}$ hold. The orientation of the maximum principal stress (hence, of the material symmetry axes) to the global reference system is locally defined by a triplet of Euler angles (θ_1, θ_2, θ_3) - see Figure 1.

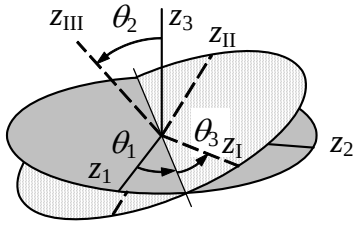

Figure 1. Euler's angles defining the orientation of the principal stresses to the global reference system

The elastic properties of the equivalent orthotropic material along its symmetry axes can be related to those of the isotropic no-tension material through a generalization of the so-called SIMP material model (see e.g. [6]), such that:

$$\begin{aligned} &\tilde{E}_1 = \rho_1^p E, \quad \tilde{E}_2 = \rho_2^p E, \quad \tilde{E}_3 = \rho_3^p E, \\ &\tilde{G}_{12} = \sqrt{\rho_1^p \rho_2^p}\,\frac{E}{2(1+\nu)}, \quad \tilde{G}_{23} = \sqrt{\rho_2^p \rho_3^p}\,\frac{E}{2(1+\nu)}, \quad \tilde{G}_{31} = \sqrt{\rho_3^p \rho_1^p}\,\frac{E}{2(1+\nu)}, \\ &\tilde{\nu}_{12} = \sqrt{\frac{\rho_1^p}{\rho_2^p}}\,\nu, \quad \tilde{\nu}_{21} = \sqrt{\frac{\rho_2^p}{\rho_1^p}}\,\nu, \quad \tilde{\nu}_{13} = \sqrt{\frac{\rho_1^p}{\rho_3^p}}\,\nu, \quad \tilde{\nu}_{31} = \sqrt{\frac{\rho_3^p}{\rho_1^p}}\,\nu, \quad \tilde{\nu}_{23} = \sqrt{\frac{\rho_2^p}{\rho_3^p}}\,\nu, \quad \tilde{\nu}_{32} = \sqrt{\frac{\rho_3^p}{\rho_2^p}}\,\nu, \end{aligned} \tag{3}$$

where E and ν are the Young's modulus and the Poisson's ratio of the isotropic material, respectively, ρ_i, *i*=1,2,3, are nondimensional variables ranging between $\rho_{\min}$(> 0) and 1, which can be interpreted as "normalized material densities" along $\tilde{z}_1$, $\tilde{z}_2$ and $\tilde{z}_3$, and *p* is a penalization parameter (usually taken equal to 3). The normalized densities are given a strictly positive lower bound, $\rho_{\min}$, to avoid any singularity in the stiffness matrix of the body, ***K***, when a finite element discretization is adopted. The interpolation in Eq. (3) is conceived so as to provide vanishing stiffness in any direction along which a variable attains its minimum value, and basically matches the anisotropic damage law proposed in [8].

Finally, denoting by $\boldsymbol{\sigma}$ and $\boldsymbol{\varepsilon}$ the arrays of the stress and strain components in the global Cartesian reference system $Oz_1z_2z_3$, the stress-strain law in this system can be written as

$$\boldsymbol{\sigma} = \boldsymbol{D}(\rho_1, \rho_2, \rho_3; \theta_1, \theta_2, \theta_3)\boldsymbol{\varepsilon} \tag{4}$$

with

$$\boldsymbol{D} = \boldsymbol{q}\widetilde{\boldsymbol{D}}\boldsymbol{q}^T \tag{5}$$

In Eq. (5), $\widetilde{\boldsymbol{D}} = \widetilde{\boldsymbol{C}}^{-1}$ and $\boldsymbol{q} = \boldsymbol{q}(\theta_1, \theta_2, \theta_3)$ is a transformation matrix which can be written as

$$\boldsymbol{q} = \begin{bmatrix} Q_{11}^2 & Q_{12}^2 & Q_{13}^2 & \sqrt{2}Q_{12}Q_{13} & \sqrt{2}Q_{13}Q_{11} & \sqrt{2}Q_{11}Q_{12} \\ Q_{21}^2 & Q_{22}^2 & Q_{23}^2 & \sqrt{2}Q_{22}Q_{23} & \sqrt{2}Q_{23}Q_{21} & \sqrt{2}Q_{21}Q_{22} \\ Q_{31}^2 & Q_{32}^2 & Q_{33}^2 & \sqrt{2}Q_{32}Q_{33} & \sqrt{2}Q_{33}Q_{31} & \sqrt{2}Q_{31}Q_{32} \\ \sqrt{2}Q_{21}Q_{31} & \sqrt{2}Q_{22}Q_{32} & \sqrt{2}Q_{23}Q_{33} & Q_{22}Q_{33}+Q_{23}Q_{32} & Q_{21}Q_{33}+Q_{23}Q_{31} & Q_{21}Q_{32}+Q_{22}Q_{31} \\ \sqrt{2}Q_{31}Q_{11} & \sqrt{2}Q_{32}Q_{12} & \sqrt{2}Q_{33}Q_{13} & Q_{32}Q_{13}+Q_{33}Q_{12} & Q_{31}Q_{13}+Q_{33}Q_{11} & Q_{31}Q_{12}+Q_{32}Q_{11} \\ \sqrt{2}Q_{11}Q_{21} & \sqrt{2}Q_{12}Q_{22} & \sqrt{2}Q_{13}Q_{23} & Q_{12}Q_{23}+Q_{13}Q_{22} & Q_{11}Q_{23}+Q_{13}Q_{21} & Q_{11}Q_{22}+Q_{12}Q_{21} \end{bmatrix} \tag{6}$$

with

$$\boldsymbol{Q} = \begin{bmatrix} c_1c_3 - s_1c_2s_3 & s_1c_3 + c_1c_2s_3 & s_2s_3 \\ -c_1s_3 - s_1c_2c_3 & -s_1s_3 + c_1c_2c_3 & s_2c_3 \\ s_1s_2 & -c_1s_2 & c_2 \end{bmatrix} \tag{7}$$

being $c_i = \cos\theta_i$, $s_i = \sin\theta_i$, i = 1,2,3 (see also [7]).

2.2. Energy-based analysis of no-tension 3D solids

The equilibrium of any linear elastic no-tension solid can be solved distributing the equivalent orthotropic material defined in Sec. 2.1 over the body, according to the sign of the principal stresses - see also [5]. In view of a displacement–based numerical solution, the continuous formulation of the problem can be stated as follows:

$$\begin{cases} \min_{\rho_1,\rho_2,\rho_3} \frac{1}{2}\int_\Omega \boldsymbol{\varepsilon}^T(\boldsymbol{u})\boldsymbol{D}(\rho_1,\rho_2,\rho_3;\theta_1,\theta_2,\theta_3)\boldsymbol{\varepsilon}(\boldsymbol{u})d\Omega \\ \text{s.t.} \int_\Omega \boldsymbol{\varepsilon}^T(\boldsymbol{u})\boldsymbol{D}\boldsymbol{\varepsilon}(\boldsymbol{v})d\Omega = \int_{\Gamma_t} \boldsymbol{t}_0^T\boldsymbol{v}\, d\Gamma \;\forall \boldsymbol{v},\; \boldsymbol{u}|_{\Gamma_u} = \boldsymbol{u}_0 \\ \theta_1,\theta_2,\theta_3 | \tilde{z}_1 = z_I,\; \tilde{z}_2 = z_{II},\; \tilde{z}_3 = z_{III} \\ \rho_1,\rho_2,\rho_3 | \sigma_I \le 0,\; \sigma_{II} \le 0,\; \sigma_{III} \le 0 \\ \rho_{\min} \le \rho_1,\rho_2,\rho_3 \le 1 \end{cases} \tag{8}$$

In the above equation, the objective function is the elastic strain energy computed through the displacement field $\boldsymbol{u}$ over the 3D domain Ω, whereas the minimization unknowns are the fields of the "normalized material densities" ρ_i, i=1,2,3. The boundary of the domain, $\Gamma = \Gamma_t \cup \Gamma_u$, usually consists of two different parts: the former is subjected to given tractions $\boldsymbol{t}_0$, whereas the latter undergoes prescribed displacements $\boldsymbol{u}_0$. Eq. (8.2) requires that the displacement field fulfils the elastic equilibrium in Ω and along Γ, whereas Eq. (8.3) prescribes alignment of the symmetry axes of the

equivalent orthotropic material to the principal stress directions. Finally, Eq. (8.4) requires the normalized densities to define a compression-only stress state all over the domain.

Discretizing the body by a mesh of *N* constant strain tetrahedral finite elements, the proposed formulation reads as follows:

$$\begin{cases} \min \dfrac{1}{2}\displaystyle\sum_{e=1}^{N} \boldsymbol{U}_e^T \boldsymbol{K}_e\left(x_{1e}, x_{2e}, x_{3e}, t_{1e}, t_{2e}, t_{3e}\right) \boldsymbol{U}_e \\ \displaystyle\sum_{e=1}^{N} \boldsymbol{K}_e\left(x_{1e}, x_{2e}, x_{3e}, t_{1e}, t_{2e}, t_{3e}\right) \boldsymbol{U}_e = \boldsymbol{f} \\ x_{1e}, x_{2e}, x_{3e} | \sigma_{eI}, \sigma_{eII,} \sigma_{eIII} \leq 0, \\ 0 < x_{min} \leq x_{1e}, x_{2e}, x_{3e} \leq 1, \\ e = 1 \dots N \end{cases} \tag{9}$$

The objective function of the above optimization problem is the strain energy, computed over the *N* elements of the mesh from the stiffness matrices, $\boldsymbol{K}_e$, and the arrays of the nodal displacements, $\boldsymbol{U}_e$, of each element. $\boldsymbol{f}$ denotes the array of the equivalent nodal loads. The three sets of element unknowns x_{1e}, x_{2e}, x_{3e} (resp. t_{1e}, t_{2e}, t_{3e}) correspond to the material densities along the symmetry axes (resp. to the Euler's angles defining the orientation) of the equivalent orthotropic material in any finite element *e*. The above minimization problem is solved through mathematical programming [9].

Details on the numerical implementation of the problem in Eq. (9) can be found in [5]. By repeatedly calling the minimization algorithm for different values of the loads, the collapse load of the structural element can also be estimated as the value at which the slope of the curve relating the load multiplier to the displacement of a control point becomes lower than a prescribed tolerance.

3. NUMERICAL APPLICATIONS

3.1. Semi-circular arch

A semi-circular arch is first considered (Figure 2). Under plane strain conditions, or with suitable transversal constraints, the arch can be representative of any segment of a barrel vault. The arch has an internal radius ri=0.4 m, whereas the external radius re=0.5 m. A three-dimensional model is analysed through a tetrahedral-based discretization made of 8329 elements, assuming the arch to have a thickness of 0.1m. The elastic properties of the material are E = 10,000 MPa and v = 0.1. A radial pressure of 0.1 MPa acts along the external surface of the arch; a horizontal live load F, with F = 1 kN and increasing with the multiplier , is applied at approximately half of the height of the arch. This structure was originally investigated in [10] to compare the value of the collapse multiplier computed through a no-tension complementary energy formulation to the result achieved by a conventional limit analysis suggesting a four-hinges collapse mechanism and an ultimate load multiplier $_c$ = 0.272. The solid line in Figure 3 shows the diagram of the horizontal displacement of the point loaded by the horizontal force versus the load multiplier , as computed in the original reference [10] through a plane strain discretization. A much finer 3D mesh is herein implemented to capture the behaviour of the arch at incipient collapse with increased accuracy. The dotted line in

Figure 3 connects results achieved by the proposed optimization procedure for independent analyses carried out at increasing values of the parameter . A good agreement is found in the first part of the curve, whereas the ultimate value of the load multiplier for which the optimization algorithm finds convergence is not far from the value of the collapse multiplier, $_c$, predicted by limit analysis.

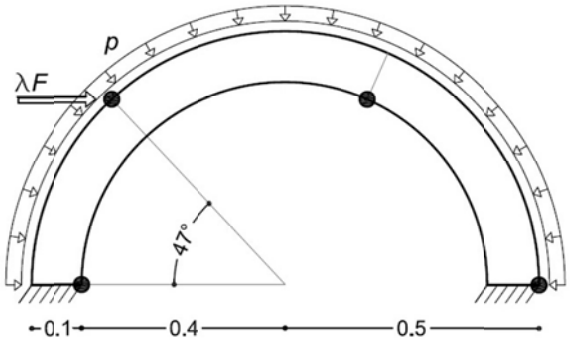

Figure 2. Semi-circular arch: geometry and load conditions

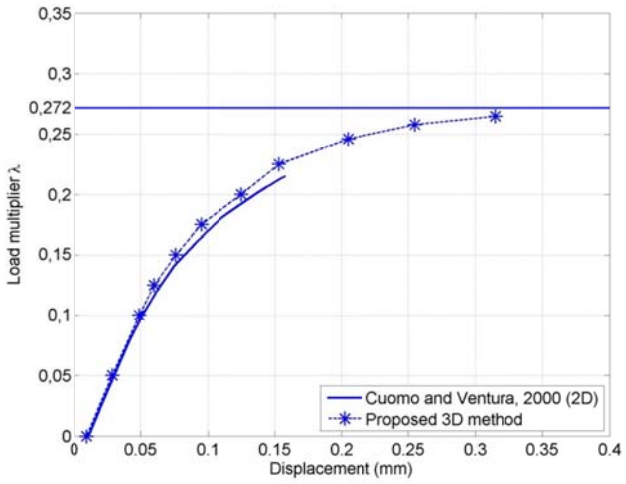

Figure 3. Semi-circular arch: load-displacement diagram obtained through the proposed numerical method vs. benchmark results [10]. The collapse load multiplier given by limit analysis is also shown

Figure 4 shows the (magnified) deformed geometry computed by the proposed procedure at incipient collapse, which matches the expected four-hinge mechanism. The highest strains are localized within limited regions of the three-dimensional domain, whereas the remaining parts of the structure exhibit an almost rigid response.

3.2. Groin vault

A groin vault given by the intersection of two barrel vaults with internal radius r_i=0.8 m and external radius r_e=1.0 m is dealt with. The material properties are assumed to be equal to those used in the previous example. A discretization with 12456 elements is employed to investigate the structural

response of the vault under the effect of self-weight, see Figure 5. Lateral confinement is enforced by suitably constraining the horizontal displacements of the sides of the vault.

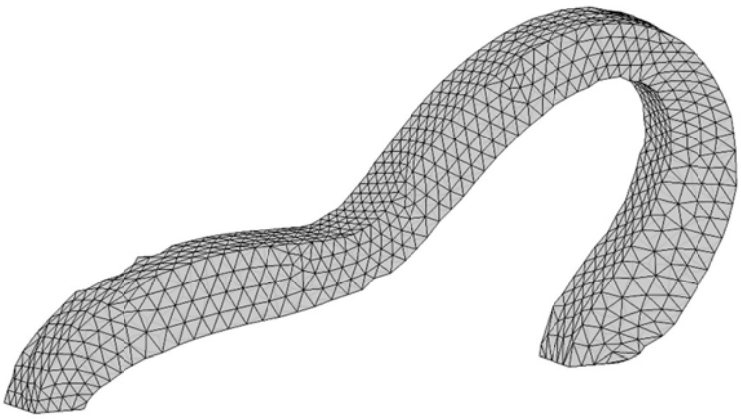

Figure 4. Semi-circular arch: magnified deformed shape at incipient collapse

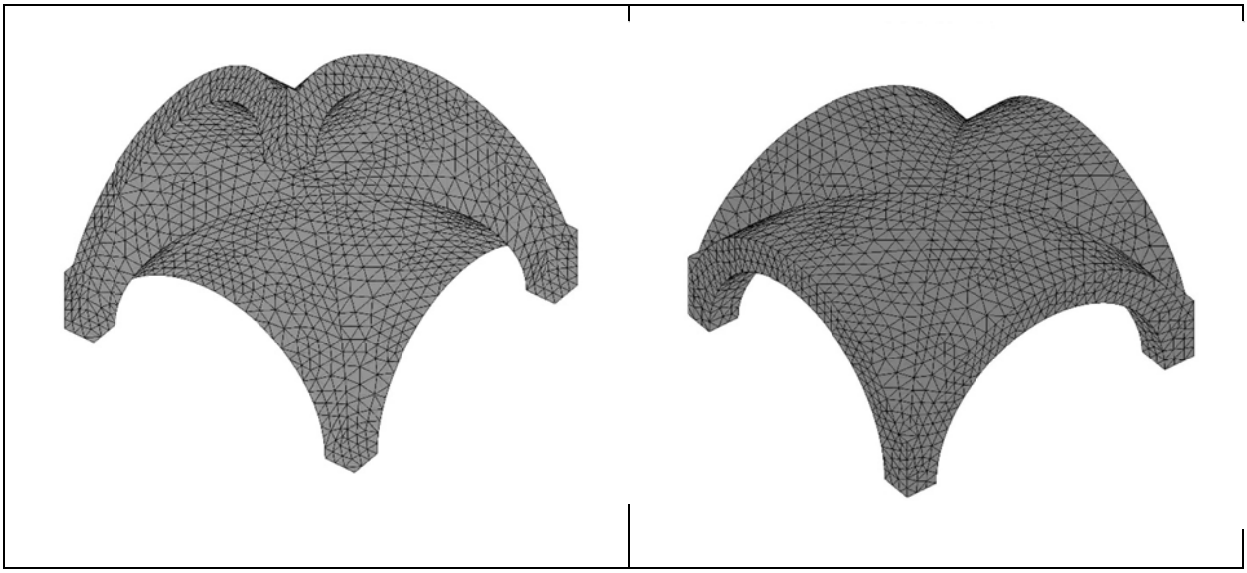

Figure 5. Groin vault: views of the adopted three-dimensional discretization

First, the vault is analysed assuming a linear elastic behaviour of the material both in compression and in tension. Figure 6 and Figure 7 show, respectively, the contour maps of the principal stresses σ_I and σ_{II}. σ_{III} is not reported here, as its order of magnitude is much lower than that of σ_I and σ_{II}. As one may easily see from the referenced figures, positive principal stresses exist both at the intrados and at the extrados, in the upper part of the structure.

The no-tension model is then adopted to investigate the structural response of the vault neglecting the tensile strength of masonry. Figure 8 and Figure 9 show, respectively, the contour maps of the principal stresses σ_I and σ_{II}, according to the results of the analysis performed through the proposed algorithm. Apparently, no tensile-stress is found in any region of the vault, whereas the maximum absolute values of the principal compressive stresses increase with respect to those obtained by a linear elastic analysis.

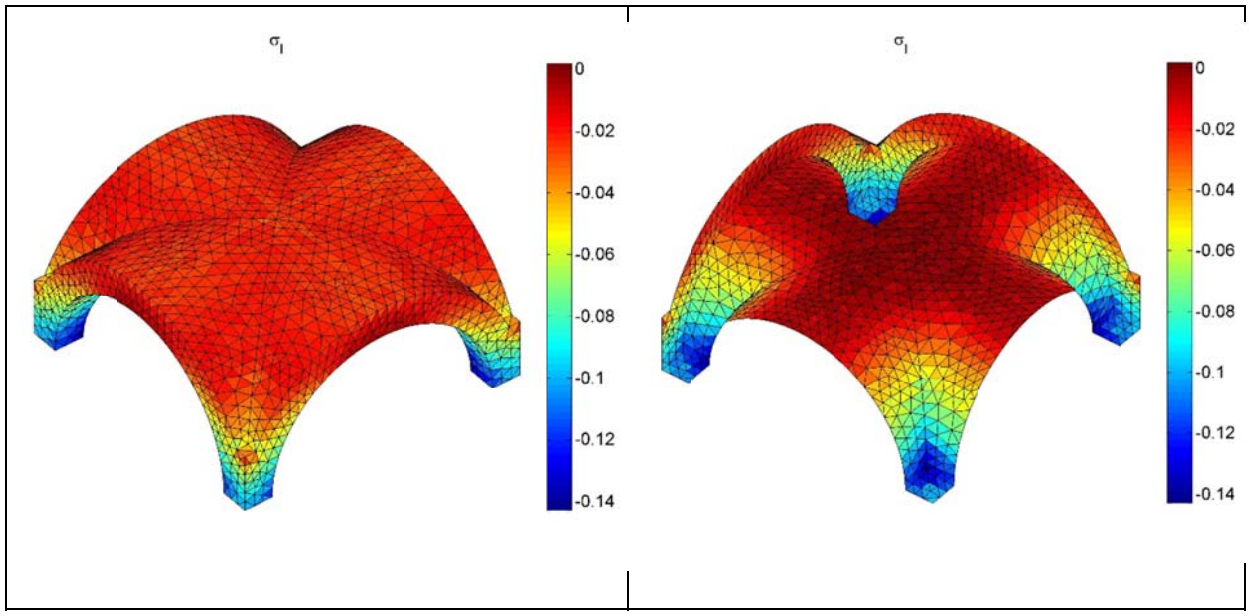

Figure 6. Groin vault: map of the principal stress σ_I (extrados and intrados, with $\sigma_I \leq \sigma_{II} \leq \sigma_{III}$) under the assumption of linear elastic behavior

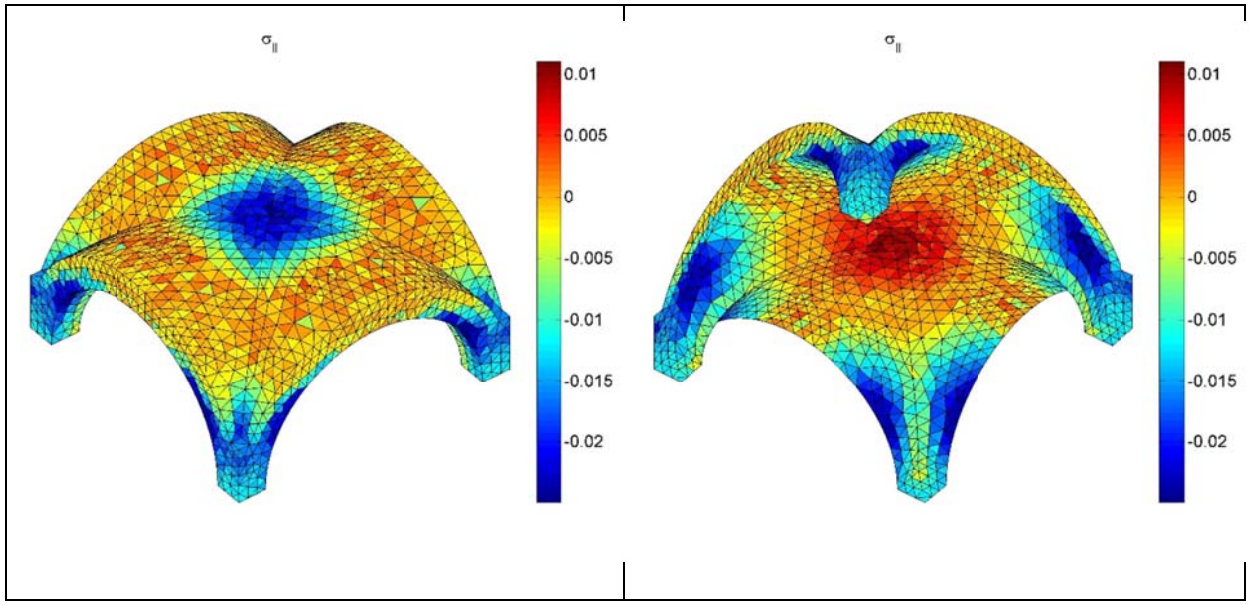

Figure 7. Groin vault: map of the principal stress σ_{II} (extrados and intrados, with $\sigma_I \leq \sigma_{II} \leq \sigma_{III}$) under the assumption of linear elastic behavior

Regions where the stress vanishes correspond to regions experiencing cracking strains. In the upper part of the intrados, the vault is fully cracked a two principal stresses vanish. At the extrados, cracks arise perpendicularly to one principal direction (corresponding to σ_{II}) in wide regions along the perimeter of the vault.

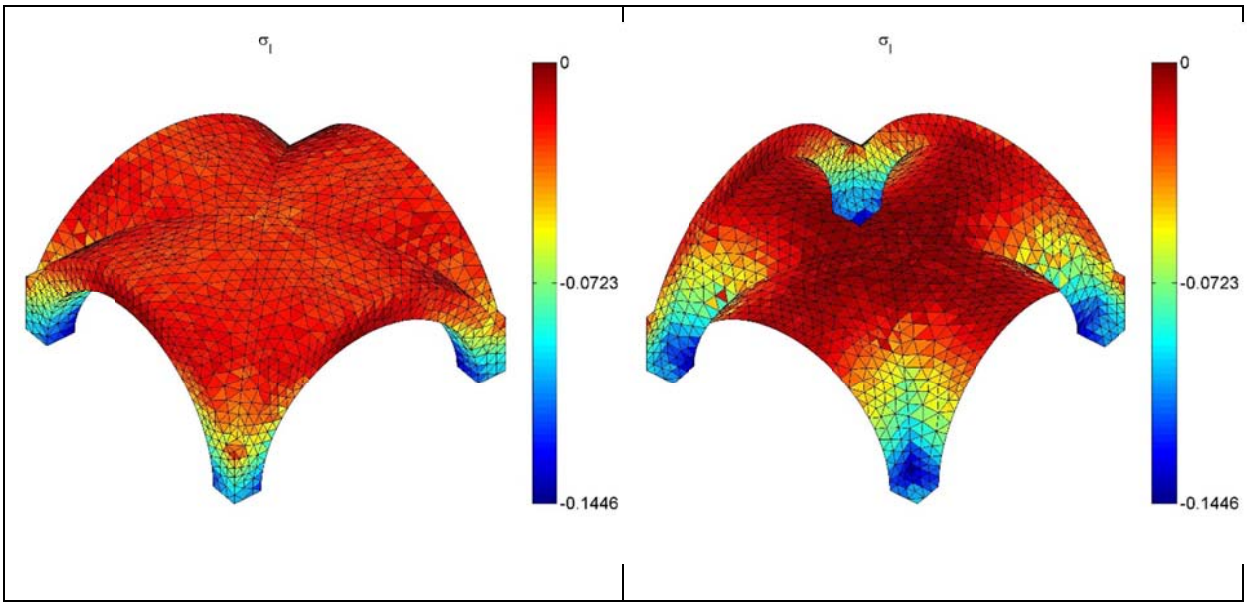

Figure 8. Groin vault: map of the principal stress σ_I (extrados and intrados, with $\sigma_I \leq \sigma_{II} \leq \sigma_{III}$) under the assumption of no-tension behavior

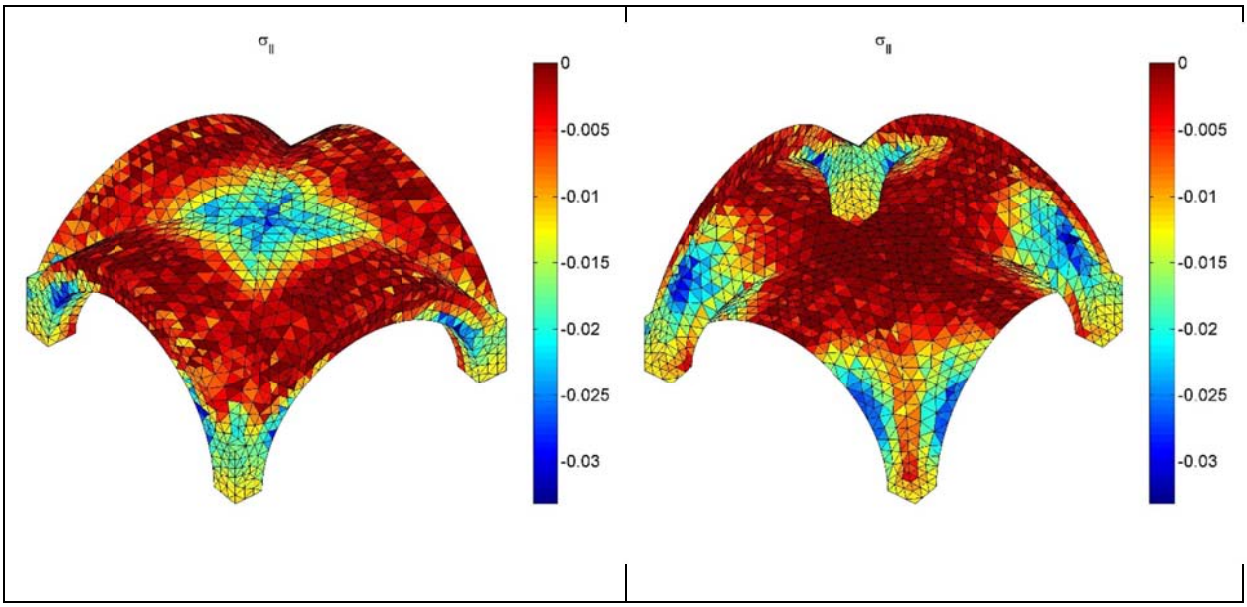

Figure 9. Groin vault: map of the principal stress σ_{II} (extrados and intrados, with $\sigma_I \leq \sigma_{II} \leq \sigma_{III}$) under the assumption of no-tension behavior

4. CONCLUSIONS

Following a recent proposal for 2D no-tension structures [5], a numerical method is presented to perform the analysis of no-tension 3D structural elements under given loads according to an energy-based non-incremental algorithm. The strain energy of a body made of an equivalent orthotropic material is minimized, so as to avoid tensile stresses throughout the structure. An interpolation typical of topology optimization [6]is employed to define the elastic properties of the equivalent material, so that a negligible stiffness is obtained along the direction(s) of the tensile principal stress(es). In the formulation implemented herein, the nondimensional “densities” that define the elastic moduli of the

equivalent material and the orientation of the relevant symmetry axes are both sets of minimization variables for the strain energy.

The proposed algorithm correctly captures the typical crack pattern observed in masonry vaults. Also, the collapse mechanisms and the collapse load multipliers of these vaults can be estimated without any a-priori hypothesis regarding the position of the "plastic hinges" (Sec. 3).

In the continuation of the work, the simplification adopted so far, according to which masonry is macroscopically isotropic, will be removed to take elastic anisotropy into account. The cracking strains predicted by the proposed approach will be also compared with those obtained by incremental analyses carried out with commercial FE (or XFE) programs. Finally, the possibility of defining optimal reinforcing layouts will be dealt with, extending the formulation adopted here to distribute the equivalent orthotropic material over the vault to define the distribution and the orientation of a tension-only strengthening layer, see in particular [11].

REFERENCES

[1] Heyman, J. (1966). The stone skeleton. *International Journal of Solids and Structures, 2, 249-279*.

[2] Lourenço, P. (2001). Analysis of historical constructions: From thrust–lines to advanced simulations. *In: Historical Constructions, P. Lourenço & P. Roca (Eds.), Guimarães, (P), 91-116*.

[3] Benvenuto, E. (1991). An introduction to the history of structural mechanics, II: Vaulted structures and elastic systems. New York: Springer.

[4] Angelillo, M., Cardamone, L., Fortunato, F. (2010). A numerical model for masonry-like structures, *Journal of the Mechanics of Materials and Structures, 5, 583-615.*

[5] Bruggi, M. (2014). Finite element analysis of no-tension structures as a topology optimization problem. *Structural and Multidisciplinary Optimization, 50(6), 957-973*.

[6] Bendsøe, M., Sigmund, O. (1999). Material interpolation schemes in topology optimization. *Archives of Applied Mechanics, 69, 635-654*.

[7] Mehrabadi, M.M., Cowin, S.C. (1990). Eigentensors of linear anisotropic elastic materials. *Quarterly Journal of Mechanics and Applied Mathematics, 43(1), 15-41*.

[8] Papa, E., Taliercio, A. (2005). A visco-damage model for brittle materials under monotonic and sustained stresses. *International Journal for Numerical and Analytical Methods in Geomechanics, 29(3), 287-310.*

[9] Svanberg, K. (1987). Method of moving asymptotes - A new method for structural optimization. *International Journal for Numerical Methods Engineering, 24, 359-373*.

[10] Cuomo, M., Ventura, G. (2000). Complementary energy formulation of no tension masonry-like solids. *Computer Methods in Applied Mechanics and Engineering, 189(1), 313–339.*

[11] Bruggi, M., Taliercio A. (2013). Topology optimization of the fiber-reinforcement retrofitting existing structures. *International Journal of Solids and Structures*, 50(1), 121-136.